Pergamon

Int. J. Heat Mass Transfer. Vol. 40, No. 3, pp. 573–588, 1997

0017–9310/97 $15.00 + 0.00

PII: S0017–9310(96)00122–6

Heat transfer and ice formations deposited upon cold tube bundles immersed in flowing water—II. Conjugate analysis

MICHAEL KAZMIERCZAK and PAUL ALEXANDER INTEMANN

Department of Mechanical, Industrial and Nuclear Engineering, University of Cincinnati, Cincinnati, OH 45221-0072, U.S.A.

(*Received* 1 *December* 1995 *and in final form* 29 *March* 1996)

Abstract—Cold tube banks were subjected to a crossflow of water. Internal cooling of the tubes below freezing resulted in gradual ice deposits to occur on the exterior of the tubes; this moving ice–water interface was then allowed to stabilize. The tube bank heat transfer rate with ice formations was examined in a global sense in Part I of this study and showed trends significantly different from the convective heat transfer rates applicable to non-icing tube bank designs. These differences could not be resolved on a global scale. Thus, the resulting ice shapes are analyzed in greater depth in the second half of this investigation, with the focus redirected locally with an initial objective to determine the *distribution* of the local convective heat transfer coefficient h_{local} along the ice–water interface. While this provided some new and interesting information, it nevertheless was still not able to explain the reasons behind the disparity. Thus, the problem was re-analyzed from a totally different perspective, as a conjugate problem. It was found that the thermal resistance of the ice layer, due to its relatively low thermal conductivity, *cannot* be neglected and becomes a controlling parameter in the problem, particularly as the ice thickness increases. In the limit, as the thickness of the ice layer vanishes, the problem is seen to reduce to one of pure convection, but, as the ice layer thickens, it quickly becomes one of conduction dominated heat transfer. Finally, the non-uniform shape (taper effect) of the ice deposits on the tubes was found to drive up the heat transfer from the tubes as compared to the heat transfer which would occur if the same amount of ice were uniformly distributed around the tubes' perimeter.

INTRODUCTION

The *global* heat transfer/ice volume characteristics of ice-on-tube systems were previously discussed in Part I. While useful and accurate correlations that describe both the energy exchange and ice volume production of such devices were developed, the convective heat transfer, when expressed utilizing standard methods historically employed for non-icing tube bank designs, behaved quite differently. The focus of Part II of this investigation is to uncover and explain the possible reasons behind the observed performance differences between ice-on-tube and non-icing tube bank designs.

The study of *non-icing* tube banks has had a very long and rich history; the early large-scale utilization of many such devices in all sectors of industry required a deep understanding of the various governing parameters which influence the performance and efficiencies of non-icing tube bank designs. Carrier and Busey [1] and Reiher [2] were in all probability the first researchers to study tubes which were assembled in repetitive pitch patterns that resembled modern tube bank designs; their experimental heat transfer data consisted of determining the mean outer convective film coefficient $\bar{h}$ as a function of freestream crossflow velocities. In 1937, Grimison [3], with particular interest in arrays of tube bundles utilized in various sections of power boilers, presented the first dimensionless correlations for staggered and in-line tube banks which were based on extensive experimental testing. These correlations expressed the average Nusselt number in terms of the freestream crossflow Reynolds number. Then, in 1950, Bergelin *et al.* [4] further expanded the existing database by experimentally studying the effect of both tube spacing and tube size; in addition they further investigated the transition from laminar to turbulent flow regime as it exists within tube banks [5]. The most recent and probably most comprehensive study of non-icing tube designs undertaken was carried out by Zukauskas and Ulinskas [6], who further expounded on the subject by experimentally determining pitch and Prandtl number effects upon the non-icing tube bank performance characteristics. The results of their study, which represents the state-of-the-art in tube bank heat transfer today, reports the tube bank's average Nusselt number as a function of three parameters: (1) the Reynolds number, (2) the Prandtl number, and (3) the tube spacing ratio. While only these particular investigations have been singled out as some of the major milestones in understanding the performance characteristics of non-icing tube banks, it should be stated that, simultaneously, many more additional studies were undertaken by other investigators. However, in

NOMENCLATURE

A	clean tube bank total exterior surface area [cm^2]
a	s_t/d
b	s_l/d
b'	s'_l/d
Bi	Biot number, $=hd/k$
d	copper tube outside diameter, 1.7145 cm
h_{local}	local convective heat transfer coefficient
h_{ave}	average of h_{local} around perimeter of ice–water interface, $=\bar{h}$
k	thermal conductivity [W m^{-1} K^{-1}]
K_f	heat transfer parameter, equation (5)
L	tube length, 12.7 cm
Nu	average Nusselt number
Pr	Prandtl number, υ/α
Q	heat transfer rate [W]
r_{tube}	tube radius, 0.85725 cm
r_{ice}	average ice radius, $=(V_{ice}+V_{tube})/2\pi L$
R	thermal resistance
R_{conj}	R_{cond}/R_{conv}, equation (10)
$Re_{d,max}$	Reynolds number, $=V_{max}\,d/\upsilon$
s_t	transverse distance between centerlines of adjacent tubes [cm]
s_l	streamwise longitudinal distance between centerlines, in-line configuration [cm]
s'_l	diagonal distance between centerlines, staggered configuration [cm]
T	temperature [K]
U_0	overall heat transfer coefficient.

Greek symbols

α	thermal diffusivity [cm^2 s^{-1}]
Θ	cooling temperature ratio, $=(T_w-T_f)/(T_\infty-T_f)$
μ	dynamic viscosity [g cm^{-1} s^{-1}]
υ	kinematic viscosity [cm^2 s^{-1}]
ρ	fluid density [g cm^{-3}].

Subscripts

cond	conduction through the ice layer
conv	convection at the ice–water interface
f	ice–water interface
row	tubes aligned perpendicular to the water crossflow
tubes	all tubes comprising a bank
w	tube surface
∞	fluid (water).

spite of the relatively large number of investigations into the *performance* aspects of tube bank heat exchangers, only a very select group of experimental studies (Zukauskas and Ulinskas, in particular) has reported the circumferential variation of the local convective heat transfer coefficient along convecting surfaces.

The number of investigations initiated to further enhance our understanding of *ice-on-tube* heat exchangers is, by comparison, even smaller. For a more thorough discussion of these studies the reader is referred to Intemann and Kazmierczak [7, 8]. Suffice it to say, most of these existing ice-on-tube bank research studies have focused their investigation of the tube's overall heat transfer rate by treating the problem as a traditional external forced convective problem. Investigators had recognized that the resulting non-uniform ice–water interface contour surrounding tubes would *somewhat* affect the variation in the local convective heat transfer coefficient distribution, but that otherwise the problem would remain essentially the same as that of non-icing tube banks. While at first this reasoning may seem logical, the results obtained in Part I of this study showed that the global heat transfer rate of tube banks with ice deposits changes so drastically from that of a non-icing tube bank configuration that other causes have to be responsible. Part II of this study starts by examining the effect which the ice layer has upon the *local* convective heat transfer coefficient of a tube surrounded by ice that is located within an ice-on-tube bank configuration. It then shifts gears, adopting a totally different point of view, upon the realization that the appearance of ice deposits on the tube's exterior instantaneously changes that solid–liquid interface boundary condition from one of an isothermal state to a non-uniform heat flux boundary condition, and then re-addresses the problem again, but as one of *conjugate* heat transfer.

EXPERIMENTAL DATA

The same experiments used to investigate the global behavior of ice-on-tube bank designs in Part I are further analyzed here in Part II to study the local convective heat transfer characteristics.

METHOD OF ANALYSIS

The finite element analysis approach previously outlined in Part I of this study [8] was also used to locally analyze the steady-state ice shapes which developed within tube bank geometries. All end-view ice shapes were documented photographically; then scanned and digitized and finally input into a standard finite element code, which then solved the two dimensional heat conduction equation within the ice annulus. The output from these FEA runs which were most

pertinent to the local interface heat transfer analysis were (1) the total ice volume which was deposited upon each tube, and (2), the local convective heat transfer film coefficient h_{local} along the perimeter of the ice–water interface, based upon the ambient free-stream crossflow water temperature and on the actual surface area of the ice interface. Part II's attention was aimed more locally, at deciphering the information contained within the distribution of the local ice–water interface convective heat transfer coefficient.

RESULTS AND DISCUSSION

The local convective heat transfer film coefficients at the ice–water interface were calculated from the local conduction heat flux given by the FEA model by utilizing a surface energy balance at the interface. These results were then compared to data applicable to non-icing tube bank investigations; for this, the most recent and accurate data obtained by Zukauskas and Ulinskas [6] were used.

Staggered tube bank

The local heat transfer results reported by Zukauskas and Ulinskas for non-icing tube bank configurations show that both the magnitude and shape of the local convective film coefficient distribution around the tubes is highly dependent upon its location within the tube bank. As a comparison of the heavy solid lines in Fig. 1a and 1b clearly shows, tubes located in the first row of a tube bank exhibit a significantly lower overall magnitude in h_{local} at comparable Reynolds numbers (not the scale change). In addition, the shape of h_{local} as one proceeds around the perimeter of a tube is drastically altered by the location of the tube; the local convective film coefficient remains essentially constant from the forward stagnation point up to the 40° mark along the tube's surface when it is located in Row 1, while the h_{local} along a tube located in the interior of a tube bank is seen to immediately decrease from the maximum at the stagnation point.

Now, when comparing the results of the current study (data symbols) to these local convective heat transfer coefficients for non-icing tube bank configurations, the overriding and major conclusion which immediately stands out is that the impact of the ice deposits upon h_{local} is always highly negative, as can be seen from Fig. 1 for the staggered tube bank and Fig. 2 for the in-line configuration, i.e. the magnitude of both h_{local} and thus $\bar{h}$ is severely depressed by the presence of the ice layer. All data plotted in Fig. 1 are for a crossflow Reynolds number of 300 (based on the bare tube diameter) and for a range of Θ values, and with the exception of the 300/8 experiment, none of the data is seen to even approach the local convective heat transfer distributions (solid lines) reported by Zukauskas and Ulinskas [6] for non-icing tube banks at a much lower Reynolds number of 100. Only the 300/8 experiment has an h_{local} contour along the ice–water interface which somewhat begins to resemble that reported by Zukauskas and Ulinskas [6] at a Reynolds number of 530 (dashed line in Fig. 1a), but at a magnitude level that more closely corresponds to Zukauskas and Ulinskas [6] experiments run at a Reynolds number of 100. Figure 1a also shows that, when compared to the h_{local} contours reported for staggered non-icing tube banks, the separation point of the external flow field from the solid–liquid interface is delayed; i.e. h_{local} exhibits its minimum value further along the perimeter of the ice–water interface than has been previously observed on tubes located in non-icing tube bank configurations. Also, an increase in Θ, while holding Reynolds number constant, is seen to result in an upstream migration of the flow separation point. While Fig. 1a represents data for tubes located in the *first row* of a staggered tube bank configuration, the same basic performance is generally observed for the tubes which are situated in the *interior* of such banks (Fig. 1b). Once again, the magnitude of h_{local} is severely depressed as compared to non-icing tube banks. The separation point of the fluid from the ice–water interface now seems to have relocated somewhat upstream (120–140°), when compared to tubes located within the first row (Fig. 1a), to approximately the same perimeter location at which flow separation occurs from interior tubes of staggered *non-icing* tube bank configuration.

In-line tube bank

Examining the local convective heat transfer coefficient distributions on tubes located in *Row* 1 of in-line tube bank layouts (without icing) vs the staggered tube bank h_{local} distribution shows that similar behavior trends exist between the two different geometries at comparable Reynolds numbers (compare solid line in Fig. 1a with solid line in Fig. 2a and note the change in scale). The same can not be said for a tube located in the *interior* of an in-line tube bank configuration; now the distribution of h_{local} is seen to start low at the forward stagnation point and gradually rise along the tube surface to a maximum at roughly 65°, after which it slowly begins to drop, falling to roughly the same magnitude in the wake region. This behavior is very different from that of an internal tube in a staggered configuration where, as mentioned before, the maximum h_{local} is seen to occur at the forward stagnation point and then diminishes. Finally, as can be seen from comparing the heavy solid lines in Fig. 2a and b, note that the overall magnitudes of h_{local}, at comparable Reynolds numbers, between a row 1 and row 3 tube are very similar, in sharp contrast to the results previously discussed for staggered tube bank designs.

Now, turning our attention to the in-line ice-on-tube experiments (data symbols), the general trends in h_{local} which were observed for the staggered ice-on-tube bank experiments were also evident for the in-line ice-on-tube configuration; Fig. 2 shows the local h variations along the perimeter of the ice–water inter-

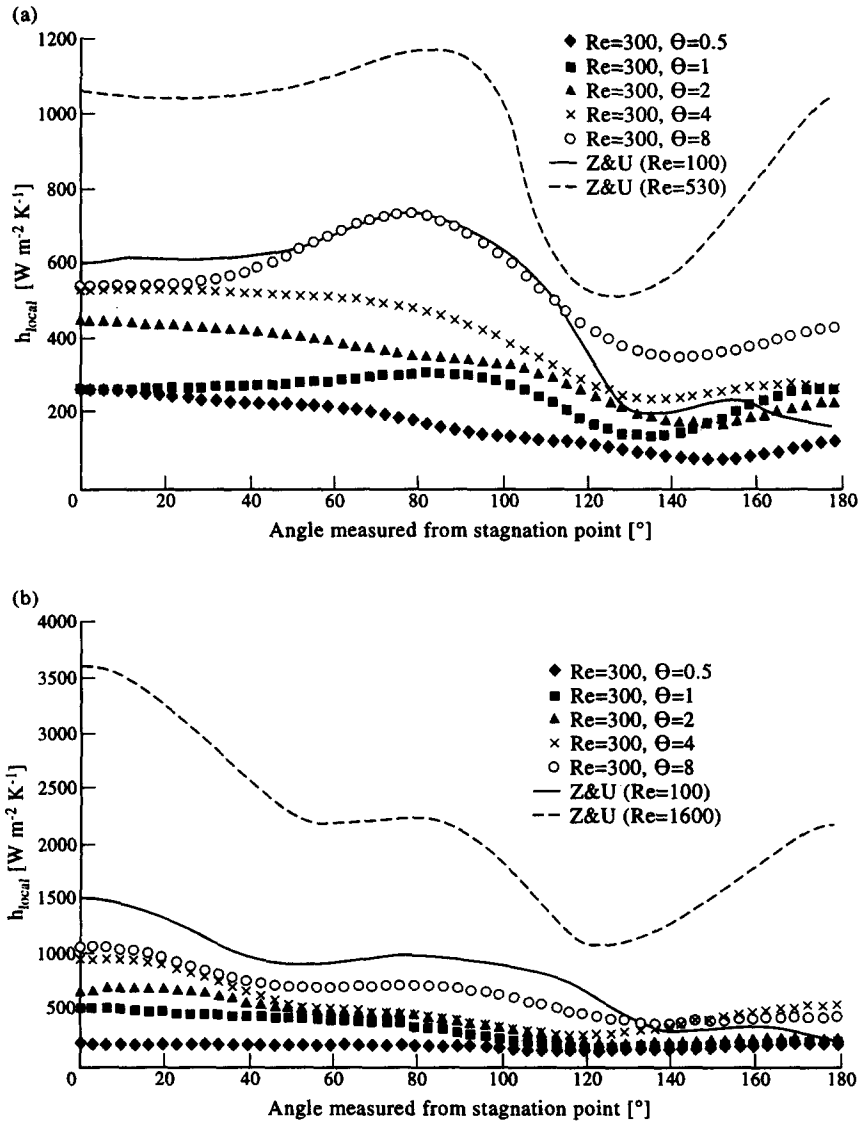

Fig. 1. Staggered tube bank configuration, local convective heat transfer coefficient, icing vs non-icing results at $Re_{d,max} = 300$. (a) Row 1 tube, (b) row 3 tube.

face. Once again, the magnitudes of h_{local} are severely depressed compared with the results reported for the non-icing in-line tube bank designs. As Fig. 2 shows, tubes located within both the first row and the interior of an ice-on-tube bank really only begin to show an h_{local} variation similar to the non-icing results at large Θ values, and even then the absolute magnitudes of h are much lower. Interestingly, the flow separation trends for tubes in the in-line ice-on-tube configuration are opposite to those previously described for row 1 tubes in the staggered ice-on-tube bank experiments. Now, the flow separation point for row 1 tubes seems to migrate rearward along the ice–water interface as Θ increases (Fig. 2a), while the interior tube's flow separation points seem generally unaffected by the magnitude of Θ (Fig. 2b), but are at a position noticeably further downstream (roughly 145–150°) compared to the staggered arrangement.

Summary of h_{local} analysis

Clearly, the single most significant effect which the ice deposits have on the tubes' local convective heat transfer coefficients is upon their magnitude, which is devastating; this is true regardless of the tube bank configuration, be it staggered or in-line, or the relative spatial location of a tube within the bank's geometry. The observed trends indicate that increasing Θ will slowly raise the magnitude of the local convective heat transfer coefficients along the ice–water interface; but not nearly to the level one would expect knowing the value of h_{local} in non-icing tube bank designs. These very low h_{local} values which are seen to exist at the

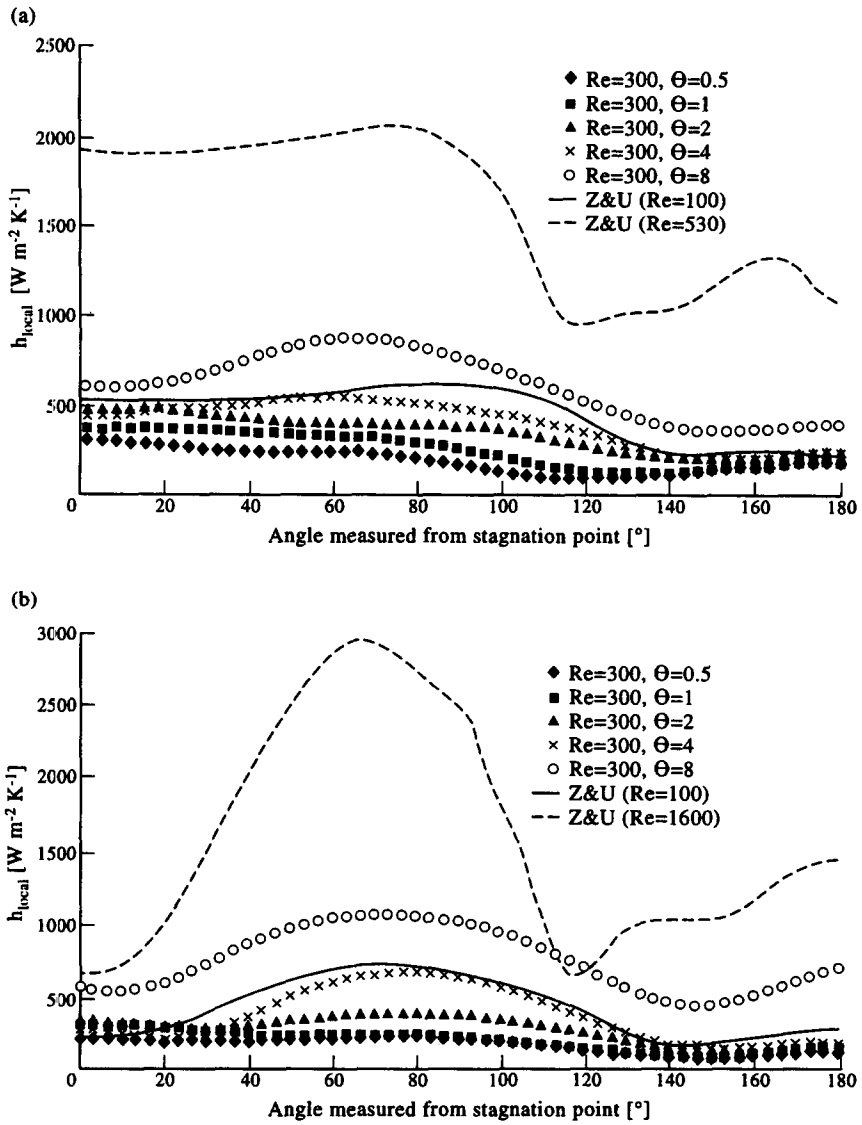

Fig. 2. In-line tube bank configuration, local convective heat transfer coefficient, icing vs non-icing results at $Re_{d,max} = 300$. (a) Row 1 tube, (b) row 3 tube.

ice–water interface surfaces (and thus low $\bar{h}$) readily explain the overall reduction in the K_f values which were reported for some of the experiments in Part I of this study. On the other hand, recall that some of the freezing experiments discussed in Part I showed K_f values which fell *above* the Zukauskas and Ulinskas non-freezing baseline correlations; this apparent dichotomy between suppressed h_{local} values and a simultaneous increase in K_f for these experiments lies strictly in the methodology used in defining K_f. To clarify, K_f was calculated (see equations (2) and (3)) based purely upon the surface area of the bare tubes and *not* on the actual ice–water interface areas used in the FEA analysis for those particular steady-state experiments. For those experiments, the value of K_f was seen to gradually increase with Θ at constant Reynolds numbers, primarily because the 'area' utilized in the denominator of equation (2) remained fixed, while the heat transfer Q in the numerator would continue to rise. This increase in Q with Θ, which is partially explained by the h_{local} trends depicted in Figs. 1 and 2, will also be driven by the simultaneous increase, primarily at low Reynolds numbers and large Θ values, in the ice–water interface *area*; these two contributing factors are seen to ultimately combine for some of the cases to the point where the overall heat transfer rate is *above* that of the baseline non-icing tube bank reference datum shown in Figs. 3a and 4a. This theory involving h_{local} and A_{ice} is substantiated by the data presented in Table 1. There, the h_{local} variations presented in Figs. 1b and 2b were used, together with the local ice interface surface area, to numerically evaluate the integral $\int h \, dA = \bar{h} A_{ice}$ for the data in those two figures, and these results were then

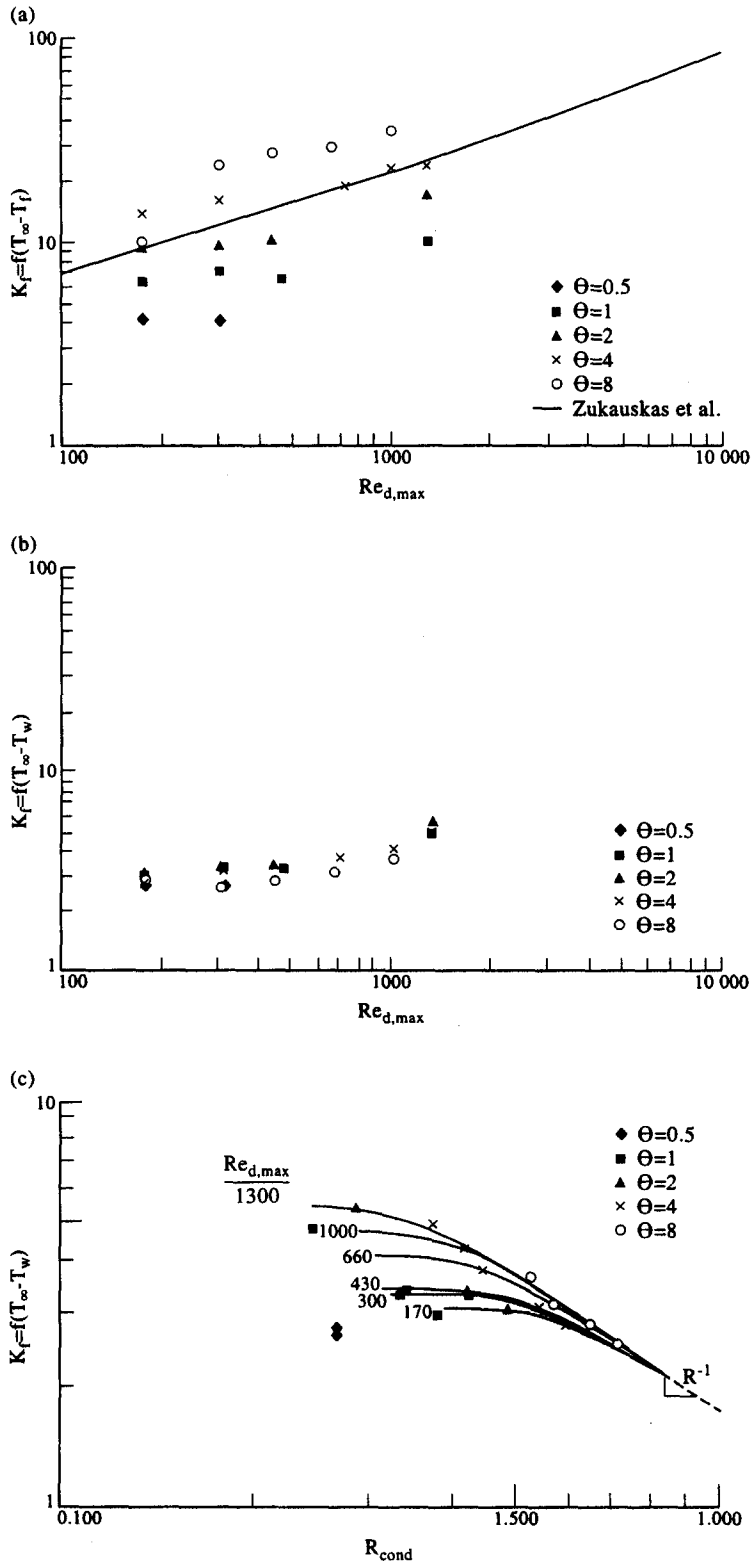

Fig. 3. Staggered tube bank configuration, heat transfer results. (a) Convection analysis, (b) conjugate analysis, plotted as function of $Re_{d,max}$, (c) conjugate analysis, plotted as function of R_{cond}.

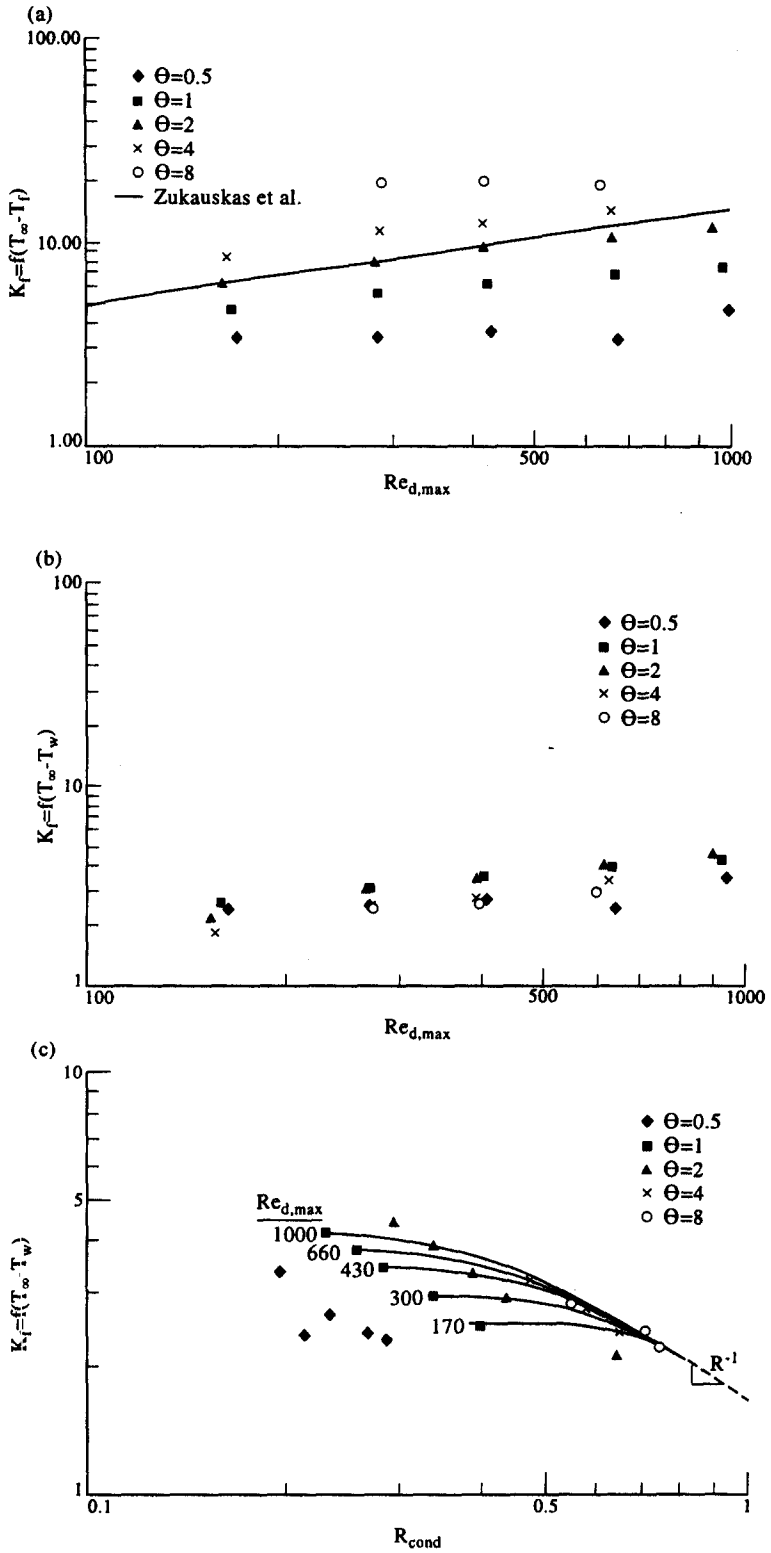

Fig. 4. In-line tube bank configuration, heat transfer results. (a) Convection analysis, (b) conjugate analysis, plotted as function of $Re_{d,max}$, (c) conjugate analysis, plotted as function of R_{cond}.

Table 1. Effect of ice layer on row 3 tube heat transfer

$Re_{d,max}/\Theta$	$\bar{h}A_{ice}$ (W/K)	$\Delta\%\bar{h}A_{ice}$	$\bar{h}$ (W m^{-2} K^{-1})	$\Delta\%\bar{h}$	A_{ice} (m^2)	$\Delta\%A_{ice}$
(a) *Staggered tube bank*: $\bar{h}A_{tube}$ at $Re_{d,max}$ = 300 (Zukauskas and Ulinskas) = 6.615 W K^{-1}						
300/0.5	1.69	−74.4	148.62	−84.6	1.14×10^{-2}	66.7
300/1	3.40	−48.6	268.28	−72.3	1.27×10^{-2}	85.2
300/2	5.12	−22.6	360.69	−62.7	1.42×10^{-2}	107.4
300/4	8.29	25.3	425.02	−56.1	1.95×10^{-2}	185.2
300/8	13.12	98.4	551.00	−43.0	2.38×10^{-2}	248.1
(b) *In-line tube bank*: $\bar{h}A_{tube}$ at $Re_{d,max}$ = 300 (Zukauskas and Ulinskas) = 4.854 W K^{-1}						
300/0.5	1.67	−65.5	149.16	−79.0	1.12×10^{-2}	64.1
300/1	2.79	−42.5	215.90	−69.6	1.29×10^{-2}	89.1
300/2	4.42	−9.0	288.98	−59.3	1.53×10^{-2}	123.4
300/4	7.00	44.2	357.95	−49.6	1.96×10^{-2}	185.9
300/8	14.51	198.9	762.66	7.5	1.90×10^{-2}	178.1

Note: all Δ% relative to Zukauskas and Ulinskas non-freezing tube bank correlations.

compared to $\bar{h}A_{tube}$ based upon the Zukauskas and Ulinskas non-icing correlations evaluated at a Reynolds number of 300. Column 3 of that table shows a percentage comparison between these results, they clearly show that at low Θ values the ice surface area is not sufficient to recoup the losses in h_{local} due to the ice deposits, but that as Θ increases, the ice surface area more than compensates for the relatively low h_{local} distributions observed. Columns 4 and 6 isolate the individual contributions of the terms comprising the data presented in column 2; column 4 clearly shows that an increase in Θ will result in a gradual rise of h with constant Reynolds number, but to magnitudes which are still significantly less than those of non-freezing tube bank designs (see column 5). Conversely, column 6 shows that the ice area will increase rapidly with Θ and is thus sufficient to offset the low h values reported in column 4; column 7 also shows the percentage increase in the ice surface area relative to the bare tube surface. In summary, the results of Table 1 show that, for both the staggered and the in-line tube bank configurations, the ice interface area increase, together with the slowly rising h values, results in a dividing line between decreasing and increasing heat transfer, relative to the non-freezing baseline, roughly in a Θ range between 2 and 4.

REDEFINING THE PROBLEM

Although it has been shown that the ice build significantly increases the surface area available for convection, in some cases to the point where the heat transfer rate is now higher than the bare tube without ice, the question which still remains is: why is h_{local} so drastically affected by the ice deposits? A closer inspection of the operating principles behind non-icing tube bank heat exchangers may reveal the answer. Commonly, tube bank heat exchangers used for industrial applications consist of tube bundles, arranged in either a staggered or an in-line configuration, which are inserted into a volume occupied by a forced crossflow; the design objective being to maximize the heat (energy) transfer between the fluid flowing through the tubes' interior and the fluid flowing around the tubes' exterior. This energy exchange between the two fluids is maximized by *minimizing* the total thermal resistance opposing the heat transfer; in a tube bank heat exchanger this total resistance includes: (1) the convective resistance to heat transfer between the interior flow and the tubes' inside surfaces; (2) the conductive resistance to heat moving radially through the tube walls; and (3) the convective resistance to heat transfer between the exterior flow and the tubes' exterior surfaces. The sum total of these three resistances effectively controls the heat transfer capabilities of common non-icing tube bank designs.

Typical non-icing tube bank designs (outer convection is limiting resistance)

As discussed above, the overall heat transfer capabilities of crossflow tube bank configurations are limited by the total thermal resistance which separates the 'hot' and 'cold' media. To this end, and to reduce the conduction resistance to heat transfer through the solid tube walls, such heat exchangers usually utilize tubes made from materials with high thermal conductivities. Likewise, to achieve the highest possible convective energy exchange along the interior of the tubes, various methods are used to ensure that the internal convective resistance is small, i.e. large h magnitudes are obtained by either relying on internal evaporation/condensation of the fluid (as found in air-conditioning systems and boilers) or, in the case where the outer fluid is air, by simply relying on forced internal circulation of *liquids* to provide the relatively high h values compared to those existent on the gas side. Thus, by minimizing two out of the three thermal resistances opposing the heat transfer between the two mediums, the performance limitations of non-icing tube bank heat transfer designs are often set by the outer convective heat transfer coefficients which exist at the interface between the exterior tube surfaces and the surrounding fluid flow. Any increase in the outer convective heat transfer coefficients will therefore

result in a direct increase in the heat transfer through the tube bank, thus many times, this h_{outer} becomes the limiting and most important parameter in predicting the performance capabilities of such tube bank designs.

Given this information, it should come as no surprise that correlating equations historically developed for tube bank designs where the thermal resistances of the solid tubes and the fluid traversing the interior of the tubes are essentially negligible, have expressed the *overall* tube bank's performance, and their heat transfer capabilities based only upon the external flow convective resistance parameters. The most widely accepted method today to describe the heat transfer characteristics of such external-flow, convection-limited tube banks has utilized equations of the form:

$$Nu = f(Re_{d,max}, Pr, a/b \text{ or } a/b') \quad (1)$$

where the average convective heat transfer coefficient $\bar{h}$, which effectively defines the mean Nusselt number, is dependent upon both the magnitude and properties of the freestream flow, which is functionally described by both the freestream Reynolds and Prandtl numbers. Equation (1), together with the temperature difference between the exterior tube surface and the freestream flow, may then be utilized to calculate the overall heat transfer rate through a given tube bank design. Thus, the heat transfer capabilities of many tube bank designs become *only* a function of the rate of convective heat transfer which is occurring at the outer tube–crossflow interface. Once again, it must be re-iterated that correlating equations such as those represented by equation (1) are only reasonable for tube bank designs where the energy exchange between the fluids is predominantly controlled by the outer convective thermal resistance between the tubes and the freestream flow.

Ice-on-tube bank configurations (combined convection–conduction resistances limit heat transfer)

From an equipment manufacturer's standpoint, a traditional non-icing tube bank design is readily adaptable for conversion into an ice-on-tube bank arrangement; only relatively close-packed tube bank designs, due to their propensity to exhibit almost immediate ice bridging between adjacent tubes, are probably not suitable for such a conversion and thus should be avoided. By sub-cooling the temperature of the fluid that is circulated throughout the interior of the tubes, to below that of the freezing temperature of water, some of the crossflow water that surrounds the tubes will begin to solidify, causing ice to be deposited on the tubes' exterior surfaces. While this appearance of an ice coat on the exterior surfaces at first may seem to be a rather minor change, the effect it has on the overall heat transfer capabilities of the tube bank can be rather profound. The introduction of an ice layer adds an additional thermal resistance to the heat flow, thereby completely altering the very simple, well-established problem statement relating to non-icing tube bank configurations as discussed above. Due to the relatively low thermal conductivity of ice, its k value being approximately 200 times less than that of copper, the previously convection limited problem is redefined to one which is now controlled by the combined convection–conduction resistances. Furthermore, note that the ice layer also results in the outer convection surface boundary condition to *change from an isothermal state*, generally applicable when the internal resistances due to convection inside the tube and conduction through the solid are all negligible, to one of a constant (steady-state) spatially non-uniform *heat flux boundary condition*, whose level and distribution is dictated by the rate of the local heat flux conducted through the ice annulus at a given point along the ice–water interface. The fact that the solid–liquid interface temperature of the ice-on-tube bank design is known to be at 0°C is merely a consequence of the local phase equilibrium and is purely coincidental, it does *not* imply the existence of an isothermal wall boundary condition in the usual sense, a surface at a uniform temperature which is situated on *an infinite heat sink or source*. Thus, to develop correlations for ice-on-tube bank designs similar in form to those developed for non-icing tube banks would be convenient, but only relates part of the story. Clearly, the appearance of an ice layer which coats the tubes transforms the previous convection-limited problem into one which is totally different, and much better described as a combined convection/conduction (i.e. conjugate) heat transfer problem.

CONJUGATE PROBLEM ANALYSIS

Many practical convective heat transfer problems can be described using the idealized *isothermal* boundary condition, that is, the thermal conductance of the solid wall contacting the fluid is assumed *infinite*, and thus the problem is attacked by determining a surface convective heat transfer coefficient based purely on the prescribed freestream and temperature conditions. Such is the case for highly conductive non-icing tube bank configurations with negligible internal convective film resistances. Conversely, convective heat transfer which occurs alongside solids that exhibit a *finite* thermal conductance has historically been known as a conjugate problem, where now the heat transfer rate at the solid–liquid interface is governed by the simultaneous interaction between the conduction in the solid and the external flow field's fluid motion. Thus, while a non-icing tube bank design constructed with high conductivity tubes (and with 'infinite' internal convection) will clearly fall into the pure convection type problem category, the appearance of an ice layer, with its relatively low thermal conductivity, upon these same tubes, will immediately redefine the problem into one classified as a conjugate type.

Convection limited vs conjugate behavior

Recall, in Part I of this study, that the experimental ice-on-tube data collected was analyzed within this framework of a pure convection-type problem in order to obtain a comparable K_f factor (based upon the temperature difference between the freestream water and the ice–water interface) and was calculated, for the test data, according to:

$$Nu = \frac{\bar{h} \times d}{k_\infty} = \frac{Q_{\text{tubes}} \times d}{k_\infty A(T_\infty - T_f)} \tag{2}$$

and then

$$K_f = \frac{Nu}{Pr_\infty^{0.36}(Pr_\infty/Pr_f)^{0.25}}. \tag{3}$$

A comparison between the experimental icing tube bank results defined in this manner, and the Zukauskas and Ulinskas [6] non-icing tube bank correlations was reported in Part I of this study and is, for the reader's convenience, repeated here in Part II as Figs. 3a and 4a. Clearly, as is readily apparent from these figures, the ice-on-tube data does not agree well at all with the non-icing correlations. The conjecture is that the outer convective film coefficient is totally redefined by the ice layer's low thermal conductivity and the resulting transformation of the surface boundary condition from a true isothermal state to a non-uniform heat flux condition. Thus, a conjugate analysis of the problem which includes the region of the solidified ice might be more appropriate to describe the overall heat transfer rate of the tube bank in this particular situation.

To this end, the K_f factors were recalculated for the present ice-on-tube experiments based upon the *total* temperature difference between the freestream water and the *tube wall surface* temperature, i.e. the $(T_\infty - T_f)$ term in equation (2) was replaced with $(T_\infty - T_w)$. These new 'overall' K_f factors, redefined in this manner to account for the conjugate aspect of the problem, have been re-plotted in Fig. 3b and c for the staggered tube bank geometry, and Fig. 4b and c for the in-line configuration.

The new K_f results, which are now based on the overall temperature difference and which include the temperature drop through the ice layer, when plotted as a function of the freestream Reynolds number (Figs. 3b and 4b), reveal a drastic change in the Θ and Reynolds number dependence, as compared to before, when K_f was expressed only in terms of the fluid temperature difference. The comparison shows that the Θ dependence has significantly decreased and almost disappears; the data plotted in this manner tends to, but not quite, collapse to a single line; a small Θ effect is still visible, but now the trend is reversed as compared to before (i.e. K_f *decreases* as the Θ value increases). Also, we observe by comparing Fig. 3b with a (or by comparing Fig. 4b with a) that the Reynolds number dependence has likewise diminished; in fact, for the staggered arrangement (Fig. 3b) the K_f values obtained in the low Reynolds number range appear to be fairly insensitive to $Re_{d,max}$ (i.e. horizontal line); only at elevated Reynolds numbers ($Re > 700$), when the ice layer becomes substantially thinner, does K_f become dependent upon $Re_{d,max}$.

The revised overall K_f results are also plotted in Figs. 3c and 4c as a function of the conduction resistance parameter R_{cond}, whose values represent the resistance to heat flow within the *solid region* of the problem and which we normally would expect to be an important factor in any conjugate type problem. This thermal resistance to conduction heat transfer in the ice annulus, assuming steady-state one-dimensional radial heat flow in cylindrical coordinates, is:

$$R_{\text{cond}} = \frac{\ln \dfrac{\bar{r}_{\text{ice}}}{r_{\text{tube}}}}{2\pi k_{\text{ice}} L}. \tag{4}$$

In calculating the value of this conduction parameter for our experiments, we took $\bar{r}_{ice}$ as the average ice radius, assuming the entire ice volume, determined from the FEA runs, was re-distributed uniformly over all of the tubes. Also note that, since the resultant final ice thickness is not known *a priori*, but rather is part of the solution, this parameter, unlike the wall coating thickness parameter found in other conjugate problems, cannot be independently varied. Inspecting Figs. 3c and 4c shows the effect of the R_{cond} parameter on K_f. The figures reveal that for small values of R_{cond} (i.e. relatively thin average ice layer), K_f is at essentially independent of R_{cond} and mainly depends on $Re_{d,max}$ and, to a much lesser extent, on Θ. This is clearly illustrated by the lines connecting tests conducted at the same $Re_{d,max}$ that tend toward the horizontal as R_{cond} decreases. However, Figs. 3c and 4c also reveal that, as the value of the conduction parameter increases (i.e. the ice layer gets thicker), its impact on the overall heat transfer rate in terms of the K_f number becomes stronger, in fact its influence at $R_{cond} = 0.6$ has increased to the point where R_{cond} has become the *single* most dominant parameter of the problem, subsequently causing the lines of constant $Re_{d,max}$ to converge. Also, we note that at that value, the K_f dependence on R_{cond} approaches the expected $(R_{cond})^{-1}$ power given by the pure conduction asymptote. In summary, by treating the problem as being of the conjugate type and by redefining K_f accordingly, we have shown that the ice layer thickness has a major impact on the overall system behavior and thus its influence upon the relative magnitudes of the convective and conductive thermal resistances requires further scrutiny.

Relative magnitude of convective vs conduction resistances

As the behavior in Figs. 3c and 4c showed, when analyzing the test data of ice-on-tube bank designs from a conjugate approach, the influence of the crossflow Reynolds number upon the K_f heat transfer

parameter reduces significantly as the value of the thermal conduction parameter increases. This indicates that the convective heat transfer rate which occurs along the ice–water interface is being limited, at least for some of the experiments, by the maximum heat transfer possible via conduction through the solid ice. Thus the main governing parameters which essentially control the heat transfer rates in ice-on-tube bank designs are the convective resistance at the ice–water interface, the conduction resistance of the ice layer and their relative combined contributions. To further clarify this point, the experimental data from the two inner-most tubes located in the interior of row 3 of the two test configurations were selected for further analysis. To analyze the conduction resistance of the uneven ice layers, the ice volumes around each tube determined by the FEA for the various experiments were once again converted to an effective ice radii $\bar{r}_{ice}$, a radius which, when multiplied by $2\pi L$, would yield the equivalent amount of tube-plus-ice volume obtained from the FEA runs.

As presented in any undergraduate heat transfer text, the overall heat transfer coefficient U_0 for any cylindrical heat transfer problem involving radial heat conduction across a solid wall with simultaneous convection at the outer surface, referenced to the outside surface area (and multiplied by k_{liquid}/r_{outer} to render it dimensionless) is given by:

$$\frac{k_{water}}{k_{ice}}\ln\left(\frac{\bar{r}_{ice}}{r_{tube}}\right)+\frac{k_{water}/h_{ave}r_{tube}}{\bar{r}_{ice}/r_{tube}}=\left(\frac{k_{water}}{\bar{r}_{ice}}\right)\frac{1}{U_0}. \quad (5)$$

The two dimensionless resistance terms of equation (5) are plotted against one another in Fig. 5 and show the variation of the two resistances with both Reynolds number and Θ for tubes located in row 3 of the staggered (Fig. 5a) and in-line (Fig. 5b) arrangements. The data in these figures which appear above the dashed line indicate that the convective resistance is larger under these test conditions than the conductive resistance, but, on the other hand, data that fall below the dashed line mean the opposite, i.e. that the convective resistance is now smaller in magnitude than the conductive resistance. The limiting case, where the data would fall on the vertical axis, implies a purely convective resistance-only type problem (the tube bank heat transfer rate is determined from the convection coefficient only) while, at the other extreme, data resting precisely on the horizontal axis would indicate a problem belonging to the limiting case behavior of conduction-only type problems. Also note that, in the figure, the direction of increasing Reynolds number is always towards the origin. As the Reynolds number is increased the values of both resistance parameters are reduced; the convective resistance will decrease because an increase in Reynolds number will raise h_{ave}, while the conduction resistance will decrease since an increase in Reynolds number will also reduce the ice thickness; in the limit as $Re \to \infty$ both resistances will vanish.

Inspecting the data plotted in Fig. 5 shows that the conductive resistances (as defined above using the concept of an effective ice radius) for the vast majority of experiments performed are greater in magnitude than the measured convective resistances, i.e. the data points generally fall below the dashed line. Only tests performed with the Θ parameter equal to 0.5 exhibited the opposite behavior, that is, the convective resistance outweighed the conductive resistance. As expected, an increase in Θ results in an increase in ice thickness, this in turn results in data points in which the conductive resistance exceeds the convective resistance, while smaller values of Θ, i.e. thinner ice thickness, tend to equalize this imbalance between the thermal resistances until, at Θ equal to 0.5, the convective resistance becomes the dominant factor in controlling the heat transfer. When Θ equals one, the temperature drop through the ice layer is identical to the temperature drop between the interface and the free-stream water, i.e. $(T_f - T_w) = (T_\infty - T_f)$, and hence the two resistances have nearly become equal and thus approach the diagonal dashed line. Changing the value of the Reynolds number is clearly seen in the figures to alter or modify the relative contributions of the convective and conductive resistances, yet the figures also show that, even when *Re* is varied over its entire range, it did not, for any of the experimental runs with a fixed Θ, cause the dominant resistance to switch from conduction to convection. The figures also clearly show that, not only does the value of Θ dictate which resistance will dominate, but the slope of the constant Θ lines indicates the degree to which the convection coefficient depends on the Reynolds number. For example, we see that for the staggered tube bank experiments for which Θ equals 8 (the data near the bottom of Fig. 5a), the convection coefficient is almost constant and is only very weakly dependent on *Re* over the full $300 < Re < 1000$ range tested, i.e. the slope of the $\Theta = 8$ line is nearly zero. This we feel occurs due to the fact that at $\Theta = 8$ the rate of energy transfer through the ice covered tube is essentially limited by the rate of heat *conducted* through the ice annulus and that the rate of convective heat transfer, under these conditions, is of secondary importance. However, as also shown by the same figure, the convection coefficient's dependence on *Re* becomes much stronger as the value of Θ becomes smaller (the slope of the lines of constant Θ become steeper). Also note that decreasing Θ with constant Reynolds number will simultaneously lessen the impact of the conductive resistance (ice thickness), yet it still remains a finite value for all of the experiments. Finally, comparing Fig. 5a with b shows that both staggered and in-line tube bank configurations qualitatively exhibit similar behavior.

Now, with these relative magnitudes of the competing thermal resistances in mind, the validity and purpose of developing convective heat transfer correlations for ice-on-tube banks based upon the mind-set of a dominant convective thermal resistance in

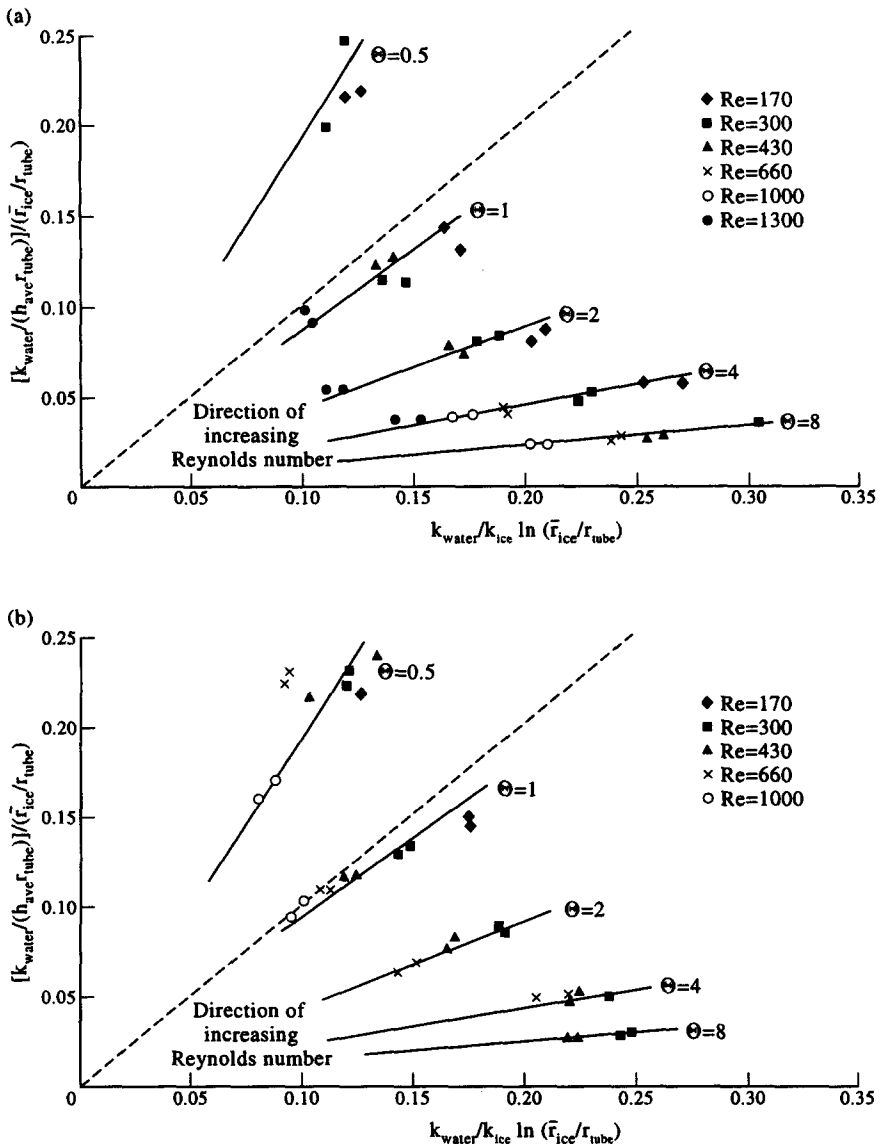

Fig. 5. Icing tube bank configuration, convective vs conductive thermal resistances for tubes located in row 3. (a) Staggered arrangement, (b) in-line arrangement.

non-icing tube banks could be called into question. On the other hand, looking at the problem from the conductive resistance perspective, some may argue that, based on the above results, ice-on-tube bank configurations would be better analyzed strictly from a conduction standpoint. Either way, one must keep in mind that the surrounding freestream flow conditions, i.e. the convection, will directly impact the location of the interface boundary location and thereby, indirectly, fix the absolute magnitude of the conductive resistance and heat transfer through the ice. Thus, it would therefore be erroneous to try to neglect this coupled convection/conduction behavior, i.e. conjugate aspect of this problem, since the ability of the ice–water interface location to literally float until a steady-state equilibrium condition between the convection and conduction heat transfer rates is obtained will *always* link the conductive resistance to the convective resistance.

Conjugate analysis concluded and taper effect

To complete the ice-on-tube bank conjugate analysis, the experimental data collected for the tubes located in row 3 of both the staggered and the in-line configurations were analyzed again, one last time. The quest this time was to find a unique *single* parameter that best describes the observed coupled convection–conduction heat transfer behavior. Now having demonstrated that both the convective and conductive resistances play a significant role in determining the overall heat transfer rate, it was obvious that this single parameter, if in fact one did exist, must be constructed in such a fashion that somehow combines the information contained in both resistance

parameters. In this spirit, a new dimensionless parameter, R_{conj} was defined, it was simply the ratio of the two resistances:

$$R_{conj} = R_{cond}/R_{conv}. \quad (6)$$

Alternatively, one may also interpret this parameter as the ratio of the conduction and convection thermal length scales; more specifically, the thickness of the ice coating over the thermal boundary layer thickness. When expressed in either manner, we see that very large R_{conj} values, $R_{conj} \gg 1$, imply that the overall thermal resistance is dominated by the conduction resistance in the ice, whereas the opposite situation exists for $R_{conj} \ll 1$, which implies that the convective boundary layer is the limiting resistance.

Before presenting the ice-on-tube results as a function of R_{conj}, it is important to point that this parameter, although heuristically developed, could have also been found by nondimensionalizing the interface boundary condition. Furthermore, one should recognize that this R_{conj} parameter basically represents a sort of Biot number for this problem. Moreover, one can show, see Intemann [9], that this parameter is also approximately equal to the Θ parameter defined previously and which appeared extensively throughout this study in connection with the discussion of earlier results. That is,

$$R_{conj} = R_{cond}/R_{conv} = Bi \sim \Theta. \quad (7)$$

In light of this, the heat transfer rate for the internal (row 3) tube, obtained from the FEA analysis of the ice shape, is plotted as a function of the Θ parameter in Fig. 6 for both geometries of interest. Note that the heat transfer rate reported in this figure was first nondimensionalized by using, as the denominator, the *conduction* heat transfer rate (based on the average ice thickness $\bar{r}_{ice}$) in the large limit as $\Theta \gg 1$, i.e. when the interface temperature approaches the freestream temperature due to negligible convective resistance, and thus is normalized by the maximum rate of heat conduction $Q_{cond,max}$ based on $\Delta T_{overall}$. The data, when plotted this way, is seen to collapse quite nicely onto a single curved line, indicating that Θ is indeed the appropriate dimensionless parameter to use in describing the normalized heat transfer rate for this conjugate problem. Note that as the value of the Θ parameter increases, this dimensionless heat transfer rate approaches, but for the given experimental test conditions *never* attains, the expected asymptote of $Q/Q_{cond,max} = 1$, which would prevail at the point when the overall heat transfer rate would be determined solely by the conduction through the ice coating. Finally, one should note from the changing slope of the curve plotted in Fig. 6 that the impact of Θ upon the heat transfer rate significantly changes; the dependence seen in this figure for $\Theta < 1$ is quite different than the behavior observed for large values of $\Theta > 1$. This marked change in the heat transfer rate Θ dependence is clearly a consequence of the dominant resistance shifting, from convection in the fluid to conduction through the solid, as the value of the Θ parameter is increased beyond $\Theta = 1$.

The single correlating equation, found to fit the data very well over the entire range of Θ tested is as follows:

$$\frac{Q}{Q_{cond,max}} = \frac{1}{1/\Theta + 1}. \quad (8)$$

It is represented by the dashed line in Fig. 6. Note that this equation also mathematically contains the expected limits for $\Theta \ll 1$ and $\Theta \gg 1$. As $\Theta \to \infty$ the pure conduction behavior becomes dominant and $Q/Q_{cond,max} \to 1$, but as $\Theta \to 0$, this indicates a vanishing temperature drop across the solid ice layer caused by either the solid region becoming infinitely conductive or, more realistically, the ice coating thickness itself becoming thinner and thinner until it finally disappears. Clearly, conduction within this imaginary infinitely thin solid layer increases without bound and therefore $Q/Q_{cond,max} \to 0$. Thus, in the limit as $\Theta \to 0$, in this case the heat transfer rate becomes *independent* of the rate of conduction, and therefore, only depends on the convective resistance; the conjugate problem in this case thereby effectively degenerates into a pure convection problem. Finally, note that this correlating equation (8) fits both the staggered (Fig. 6a) and the in-line (Fig. 6b) tube bank arrangement data equally well.

In closing, it's worth mentioning that all of the trends just identified in the last section of the present analysis dealing with the ice-on-tube bank geometries are identical to those trends reported earlier by Lim *et al.* [10], who theoretically investigated a similar problem, namely, conjugate heat transfer for the case of laminar boundary layer flow over a *flat surface* 'coated' with a solid layer of non-uniform thickness and finite k. With the exception of the obvious change in geometry (solid coats a flat plate vs ice coats a circular tube), and the fact that in this problem the thickness of the solid ice layer is an unknown quantity experimentally determined as part of the solution, while in Lim *et al.*'s problem the thickness (and shape) of the solid coating is fixed and independently specified, the two problems are quite analogous. In fact, one finds that the results of both studies very closely emulate one another when one realizes that the Θ parameter of the present study is essentially identical to the J parameter used in the former study. Detailed comparisons are not shown here but can be found in Intemann [9].

One very interesting conclusion reached by Lim *et al.* [10] in their analysis, of particular relevance to this study, dealt with the effect which the *shapes* of the coating deposits have upon the total heat transfer rate from the flat plate through the coating material. When operating under the constrains of the fixed amount of coating material, they found that the total heat trans-

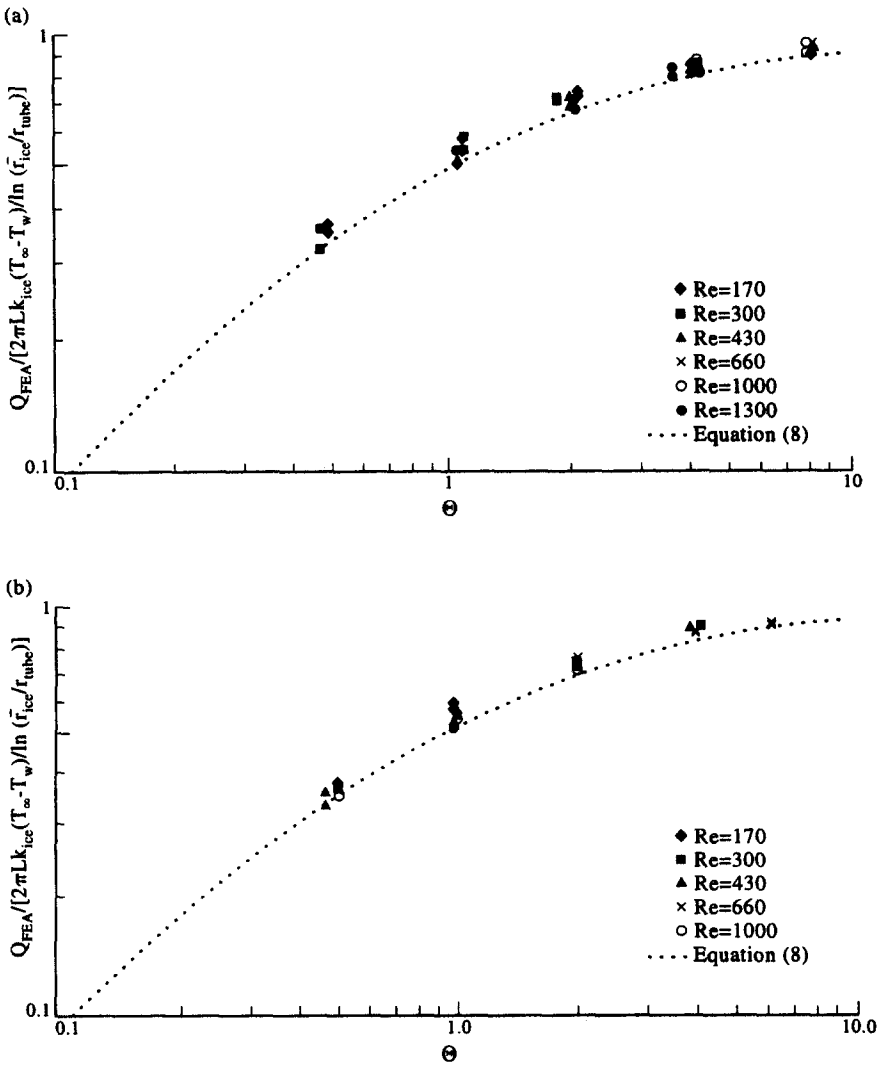

Fig. 6. Icing tube bank configuration, conjugate analysis, heat transfer vs Θ for tubes located in row 3. (a) Staggered arrangement, (b) in-line arrangement.

fer rate would *decrease* when the shape of the solid material was tapered so that its thickness decreased in the flow direction. They determined, by numerically integrating the appropriate governing equations, that the overall thermal resistance of the *conjugate* system increased as more of the material was shifted upstream toward the leading edge, thereby causing a reduction in the overall total heat transfer rate. Our data concurs with this aspect of their findings as well, but makes the point by showing that a redistribution of ice in the *opposite direction* (by positioning more ice on the aft side of the tubes, as is clearly visible in the ice shape photographs reported in Part I) leads to a net *increase* in the rate of heat transfer as compared to the case where an equal volume of ice is evenly distributed around the tube. Support for this conclusion can be found in Fig. 7, where $Q_{cond,actual}$ output from the FEA analysis of the *uneven* two-dimensional ice contours is shown, for experiments performed at a Reynolds number of 300, to be consistently higher in magnitude than the calculated one-dimensional heat transfer rates $Q_{cond(1D),\bar{r}_{ice}}$ which are based upon an even thickness distribution of identical ice volumes. As is clearly visible, these non-cylindrical ice deposits will result in the rate of heat conduction to be augmented anywhere from 1 to 12%, depending on the tube location and the Θ value, an amount comparable in size to the reduction in heat transfer reported by Lim *et al.* [10] in their conjugate analysis of nonuniformly coated flat surfaces with parallel flow. It should be noted that the general trends depicted in Fig. 7 were also observed for experiments conducted at other Reynolds numbers, but were not included in the figure for the sake of clarity. Note also that the driving temperature difference used to plot $Q_{cond(1D),\bar{r}_{ice}}$ in Fig. 7 is the temperature drop across the ice only, $T_f - T_w$, and not the overall temperature difference used to plot the results in Fig. 6.

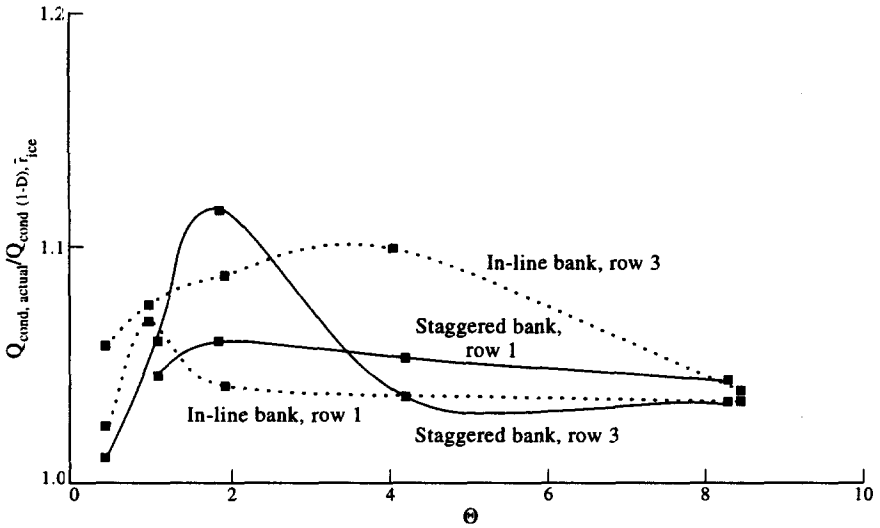

Fig. 7. Icing tube bank configuration, effect of ice taper on the rate of heat conduction through ice shapes at $Re_{d,max} = 300$.

CONCLUSIONS

The convective heat transfer results which were presented during Part I of this study raised serious questions as to the appropriateness of analyzing the heat transfer phenomenon as it occurs in ice-on-tube bank design in the same manner as one would analyze a standard non-icing tube bank configuration. Part II of the study showed that the presence of ice coatings on the tube's exterior radically influences the local heat transfer coefficients at the ice–water interface; they were found to be significantly reduced as compared with those for similar non-icing tube bank designs. These low values of h_{local} were, depending upon the value of the Θ parameter, compensated for by an increase in interface surface area, but their low magnitudes, however, could not be adequately explained from a purely convective perspective. Analyzing the ice-on-tube phenomenon as a conjugate problem revealed that the effect of the crossflow Reynolds number on the heat transfer rate of the tube bank was significantly diminished when compared to non-icing tube bank configurations. The very low thermal conductivity of ice is seen to be the main cause; this additional conductive thermal resistance is also seen to inherently alter the previous thermal boundary conditions that existed at the solid wall. Thus the problem without ice formations, which began as a pure convection problem, became one where the heat transfer is now governed by the equilibrium condition which exists between the amount of heat that can be *conducted* through the ice layer and the amount of heat *convected* at the interface via forced convection due to the crossflow. By analyzing the problem in this new light, we showed that the thermal resistance of the ice to conduct heat, especially at large Θ values when the ice layer is thick, becomes the predominant factor in controlling the heat transfer rate in ice-on-tube bank designs. Thus, it is concluded that by treating the system as a conjugate problem and including both thermal resistances, the convective resistance at the ice–water interface *and* the conduction resistance across the ice layer into the problem statement, is the most appropriate approach to take in analyzing the overall system's behavior. Plotting the total heat transfer rate as a function of the ratio of these two resistances was seen to be beneficial in illuminating the coupled convection–conduction nature of the problem and in delineating the dominant resistance. Finally, the re-proportioning of the ice thickness towards the aft perimeter of the tube was shown to increase the rate of heat conducted through the ice relative to an equi-volume layer of ice uniformly deposited around the tube perimeter.

REFERENCES

1. W. H. Carrier and F. L. Busey, Air-conditioning apparatus—principles governing its application and operation, *Trans. ASME* **33,** 1055–1136 (1911).
2. H. Reiher, Waermeuebergang von Stroemender Luft an Rohre, *VDI Z. Ver. Deutsch. Ing.* **70,** 47–52 (1926).
3. E. D. Grimison, Correlation and utilization of new data on flow resistance of heat transfer for cross flow of gases over tube banks, *Trans. ASME* **59,** 583–594 (1937).
4. O. P. Bergelin, G. A. Brown, H. L. Hull and F. W. Sullivan, Heat transfer and fluid friction during viscous flow across banks of tubes—III. A study of tube spacing and tube size, *Trans. ASME* **72,** 881–888 (1950).
5. O. P. Bergelin, G. A. Brown and S. C. Doverstein, Heat transfer and fluid friction during flow across banks of tubes—IV. A study of the transition zone between viscous and turbulent flow, *Trans. ASME* **74,** 953–960 (1952).
6. A. Zukauskas and R. Ulinskas, *Heat Transfer in Tube Banks in Crossflow*, Chap. 2. Hemisphere, New York (1988).

7. P. A. Intemann and M. Kazmierczak, Convective heat transfer for cold tube bundles with ice formations in a stream of water at steady state, *Int. J. Heat Fluid Flow* **15,** 491–500 (1994).
8. P. A. Intemann and M. Kazmierczak, Heat transfer and ice formations deposited upon cold tube bundles immersed in flowing water—I. Convection analysis, *Int. J. Heat Mass Transfer* **40,** 557–572 (1997).
9. P. A. Intemann, Steady and transient forced convective freezing experiments on subcooled tube bundles in a crossflow of water, Ph.D. thesis, University of Cincinnati, Cincinnati, OH (1996).
10. J. S. Lim, A. Bejan and J. H. Kim, The optimal thickness of a wall with convection on one side, *Int. J. Heat Mass Transfer* **35,** 1673–1679 (1992).